

PAPER View Article Online
View Journal | View Issue



Cite this: Nanoscale, 2019, 11, 8260

Two-dimensional Blue-AsP monolayers with tunable direct band gap and ultrahigh carrier mobility show promising high-performance photovoltaic properties†

Xinyong Cai, ‡^a Yuanzheng Chen, [D*‡^a Bai Sun, [Da,b] Jiao Chen, a Hongyan Wang, [Da] Yuxiang Ni, a Li Tao, Hui Wang, a Shouhui Zhu, a Xiumei Li, a Yanchao Wang, [Da] Jian Lv, [Da] Xiaolei Feng, Simon A. T. Redfern [Da] and Zhongfang Chen [Da]*

The successful fabrication of black phosphorene (Black-P) in 2014 and subsequent synthesis of layered black $As_{1-x}P_x$ alloys have inspired research into two dimensional (2D) binary As-P compounds. The very recent success in growing blue phosphorene (L'lue-P) further motivated exploration of 2D Blue-AsP materials. Here, using *ab initio* swarm-intologic ce global minimum structure-searching methods, we have obtained a series of novel and overgotically favored 2D Blue-AsP (denoted x-AsP, x = I, II, III, IV, V) compounds with As:P = 1:1 stoichic metry. They display similar honeycomb structures to Blue-P. Remarkably, the lowest-energy As^p monolayer, namely I-AsP, not any possesses a quasi-direct band gap (2.41 eV), which can be tured and direct and optimal gap for prior voltaic applications by in-plane strain, but also has an ultrahidational conficients (x_10^5 cm⁻¹). Our simulations also show that 30 nm-thick I-AsP sheet-based relishave photovoltaic efficiency as high as x_10^s , and the I-AsP/CdSe heterostructure solar cells possess a power conversion efficiency as high as x_10^s . All these outstanding characteristics suggest the I-AsP sneet as a promising material I-I-Ligh-efficiency solar cells.

Received 10th February 2019, Accepted 28th March 2019 DOI: 10.1039/c9nr01261c

rsc.li/nanoscale

^aSchool of Physical Science and Technology, Key Laboratory of Advanced Technologies of Materials, Ministry of Education of China,

Southwest Jiaotong University, Chengdu 610031, China. E-mail: cyz@cal psc org.cn bDepartment of Mechanics and Mechatronics Engineering, Centre fo. 4a. 'a...d Materials Joining, Waterloo Institute of Nanotechnology, and Depe. t of Physics and Astronomy, University of Waterloo, Waterloo, Ontario 1 21 30 ' Canada CSchool of Optoelectronic Technology, Chengdu University of Information Technology, Chengdu 610225. China

^aState Key Lab of Superhard Materials, College of Phy. . · Iilin University, Changchun 130012, China

^eDepartment of Earth Sciences, University of Combininge, Cambridge, CB2 3EQ, UK ^fDepartment of Chemistry, University of Pt. [†] Rico, Rio Piedras Campus, San Juan, PR 00931, USA. E-mail: zhongfangc'en vy. [†] il.com

† Electronic supplementary inform tic 1 (ESI) available: The convex hull for the formation energies for the different As-P stoichiometries; the optimized structural parameters of more lager. AsP polymorphs; the AIMD and DOS of the I-AsP monolayer; the capetal new of the fundamental band gap for the I-AsP monolayer, bilayer, no mayer on the in-plane stretching along the armchair direction, the zigzag cirection, and biaxial strain by the PBE level; the relationship between the energy shift of the band edge position and the dilation $\Delta l/l$, total energy shift on per surface as a function of lattice deformation along armchair and zigzag directions. See DOI: 10.1039/c9nr01261c ‡ These authors contributed equally.

Introduction

Phosphorus (P) can form various allotropes in the bulk, including black P, white P, violet P, and red P, due to inequivalent sp³ orbital hybridization.^{1,2} Very recently, a two-dimensional (2D) black P, i.e. phosphorene (Black-P), has been successfully synthesised, and is found to display a high electron mobility of ×10⁴ cm⁻² V⁻¹ s⁻¹ with a direct band gap of ~2 eV.3,4 This great achievement inspired the discovery of a series of allotropes, such as β -, γ -, δ -, ϵ -, ζ -, η -, θ -, ψ -, the octagonal tiling, tricycle-like phosphorene, and blue phosphorene (Blue-P).^{5–13} Among these 2D allotropes, Blue-P is probably most appealing due to its theoretically predicted wide tunable direct band gap (1.1 eV-2 eV), enhanced by in-layer strain and the number of layers¹⁴ and the isotropic structure. Unlike the anisotropic structure of Black-P, the in-plane hexagonal unit of Blue-P possesses isotropic structure and properties, and its bulk layer stacking is very similar to graphite. Remarkably, Blue-P has been successfully synthesized on an Au (111) substrate using molecular beam epitaxy,15 as well as on tellurium functionalized Au(111) using black P as the precursor. 16 However, Blue-P exhibits rather low carrier mobility of

 $\times 10^2$ cm⁻² V⁻¹ s⁻¹,¹⁷ which restricts its application as a photoelectric device material.

Arsenic (As), having a similar covalent radius as P among the group V elements, also exists as crystalline allotropes including black As and gray As.2 Black As is isostructural with Black P, while Gray As resembles Blue P. Their limited layers make them promising candidates for photoelectric applications, as supported by both theoretical 18-24 and experimental 25 studies. Moreover, other As allotropes, including honeycomb-structured γ -As, T-As and δ -As, are all predicted to have excellent photoelectric and thermoelectric performance. 26-29 Among these allotropes, gray As is thermodynamically most favored, and its multilayer nanoribbons have been synthesized via InAs. 17,27,30 Due to its low interlayer interaction energy, 31 it is rather easy to mechanically exfoliate gray As bulk to produce monolayer gray arsenene (Gray-As), which was recently predicted to be a semiconductor with a wide band gap (~2.5 eV)32 with high carrier mobility for optoelectronic applications.²⁹

Considering the identical 2D configurations of black-, blue-P and -As (with its exceptional properties), 2D binary black As-P and blue As-P phases provide a means to develop new materials with modulated optoelectronic properties, including improved carrier mobility. The recent success in synthesizing a limited-layer black $\operatorname{As}_{1-x} \operatorname{P}_x$ (0.17 $\leq x \leq$ 1) alloy, a promising alternative material for mid-infrared applications, ^{18,33-36} lends confidence to attempts to fabricate such 2D binary material. Meanwhile, other 2D As-P structures, mainly with As: P = 1 1 stoichiometry, such as α -AsP, β -AsP, γ -AsP, ϵ -AsP, and α -AsP have also been proposed as promising optoble tronic materials. ³⁷⁻³⁹ However, these AsP polymorphs were obtained by simply replacing alternative P atoms by As alones.

Here, to further explore 2D binary As-P compounds, we have systemically investigated the low-lying energy structures of As-P monolayer phases (As_xP_{1-x}, x 1/1,1/5, 1/4, 1/3, 1/2, 1/3, 1/4, 1/5, and 1/6) using the particle-swarm optimization (PSO) multidimensional method. 40 As such, we confirm the high stability of the As:P = 1:1 composition, and hare obtained a series of novel and energetically favorable 20 bive AsP monolayers sharing a similar honeycomb structure to Blue-P and Gray-As at this composition. More importantly, the most stable I-AsP monolayer possesses a tunable girect band gap, high absorption coefficients, ultrahigh carrier mobility, and superior photovoltaic efficiency. Compared with Blue-P, the properties of I-AsP are greatly enhanced by As merging, and some aspects are close to or even by ond those of Gray-As, suggesting that Blue-AsP is a promining material for photovoltaic applications. By following type II band alignment, we have constructed a novel so'ar cell comprising a I-AsP/CdSe heterostructure, and further demonstrate a relatively high conversion efficiency of $\sim 3\%$ in these cells.

Computational methods

By means of the multidimensional particle-swarm optimization (PSO) method implemented in the CALYPSO code, 40,41

we searched for low-lying structures of the 2D As_xP_{1-x} monolayer (x = 1/6, 1/5, 1/4, 1/3, 1/2, 1/3, 1/4, 1/5and 1/6). The validity of this method has been proved by various systems ranging from elemental to binary and ternary compounds and from the ground-state structures of 3D crystals to clusters and 2D crystals. 42-48 The geometric optimizations and electronic property computations for the 2D As-P structures were performed using the Perdew-Burke-Ernzerhof (PBE) functional in the density functional theory (DFT) framework within the generalized gradient approximation (GGA) and projector-augmented-wave (PAW), 49,50 as implemented in the Vienna ab initio simulation package (VASP). 51 A vacuum space of 20 Å was used to avoid mirror interactions of adjacent As-P freestanding monolayers. The van der Waals density functional⁵² was adopted to evaluate interlayer interactions more accurately. Monkhorst-Pack k meshes (the reciprocal space was set to be $0.025 \times 2\pi \text{ Å}^{-1}$) were selected for Brillouin zone sampling to ensure that all energy calculations are well converged to ~1 meV. The Hevd-Scuseria-Ernzerhof (HSE) hybrid functional⁵³ was employed to evaluate the electronic band structures. The dynamic stability of the 2D blue AsP monolayers was verifical chrough the direct supercell method, as implemented in the PHONOPY code.⁵⁴ The ab initio molecular dana nic; (AIMD) simulations were annealed at 300 and 750 K in the NVT ensemble, which lasted for 7.5 ps with a time step of 2.0 fs.

Results and discussion

Structures and shabilities of the blue-AsP monolayer

Both Poth as are group V elements, and can give rise to sp³ hybr diration. The covalent atomic radius of As is very close to that 21 P (covalent radii: 1.00 and 1.15 Å, respectively); thus, the pinary As-P compositions most easily form 2D crystalline structures like Black-P (Black-As) and Blue-P (Gray-As).

Based on our CALYPSO approach with first principles calculations, we comprehensively explored various possible monolayers with different As-P stoichiometries. By computing the formation energies and plotting the convex hull (Fig. S1†), we found that the energy differences among different compositions are exceedingly small, indicating that the As-P system may form an alloy. Among these stoichiometries, the As: P = 1:1 composition is thermodynamically most favorable in the 2D space. With this 1:1 composition, besides finding several typical monolayer AsP polymorphs (α , β , γ , δ , and ϵ), we also found a series of novel AsP monolayers (label as x-AsP, x = I, II, III, IV, V), and their structural parameters are given in Table S1.† To evaluate the relative stabilities of these monolayers, we computed their cohesive energies ΔE (AsP), defined as $\Delta E(AsP) = E(AsP) - E(As) - E(P)$, where E(As/P) represents the free energy of single P or As atom, and E(AsP) is that of an AsP monolayer. According to this definition, a more negative ΔE (AsP) value indicates the higher thermodynamic stability.

Paper Nanoscale

Our newly predicted I-AsP is thermodynamically most favorable; in particular, it is lower in energy than $\beta\text{-AsP}$, the previously reported lowest-energy structure (Fig. 1a). 37,38,55,56 Moreover, the cohesive energies of II-, III-, IV-, and V-AsP all are close to that of $\beta\text{-AsP}$, and much lower than that of $\alpha\text{-AsP}$ (Fig. 1b). In these x-AsP structures, both P and As atoms are three-fold coordinated with sp³ hybridization, forming buckled honeycomb hexagonal units.

Viewing these x-AsP structures from above (down onto the layers, Fig. 1c), we notice that these honeycomb x-AsP structures share extreme similarity with the atomic arrangement of Blue-P⁵⁷ (or Gray-As, ³² Fig. 1c). Viewed parallel to the layers, the puckered zigzag of these x-AsP structures in the cross-section differs significantly from the distinct armchair ridges of Black-P (or black AsP such as α -AsP, Fig. 1b) that causes the anisotropy of Black-P, which is also similar to the puckering of Blue-P (Gray-As). Thus, these x-AsP sheets can be characterized by a combined structure of Blue-P and Gray-As, which we denote "blue AsP". Among these x-AsP sheets, the I-AsP sheet is thermodynamically most stable, and is expected to be most readily achieved by experimental synthesis. Thus, in the following sections, we will focus on the I-AsP sheets.

The I-AsP monolayer contains two different hexagonal units; one consists of three neighbouring As and P atoms, and the other has three alternated As and P atoms. The unit cell consists of six atoms with lattice constants a = b = 5.96 Å. In the puckered structure, there are three types of bonds with bond lengths $d_1 = 2.52$ Å of As-As, $d_2 = 2.25$ Å of P-P, and $d_3 = 2.40$ Å of As-P, and four types of bond angles: $\theta_1 = 94.1^\circ$, $\theta_2 = 90.9^\circ$, $\theta_3 = 95.6^\circ$ and $\theta_4 = 89.2^\circ$ (Fig. 1c).

To evaluate the dynamic stability of the I-AsP monolayer, we calculated its phonon dispersion relations using the finite-displacement method. No imaginary frequency in the first Brillouin zone was found (Fig. 2a), which confirms its dynamic stability. Moreover, the thermal stability of I-AsP was examined using AIMD simulations. For $T=300\,\mathrm{K}$, the I-AsP monolayer only undergoes a minimal change, and no remarkable structural disruption is observed throughout simulations. Meanwhile, we performed AIMD simulations at 300 K under an O_2 atmosphere (Fig. S2†). After full atomic relaxation over a run of 7.5 ps, the I-AsP structure obtained from AIMD simulations at 300 K retains its initial configuration without any sign of oxidation. These simulations demonstrate that the I-AsP monolaging is stable at room temperature. When the

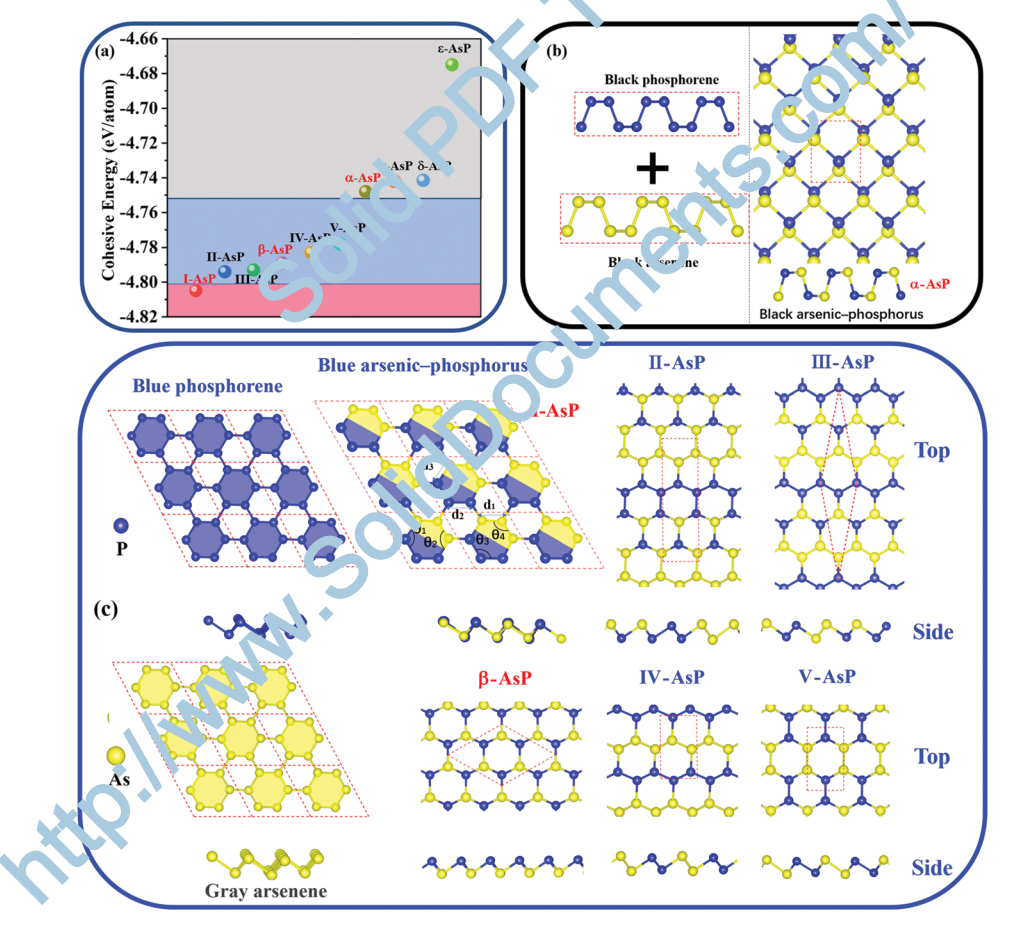


Fig. 1 (a) The computed cohesive energies of our newly predicted x-AsP (x = I, II, III, IV, V) monolayers in comparison with those of typical AsP polymorphs (α , β , γ , δ , and ε). (b) The side and top views of α -AsP as a combined structure of Black-P and Black-As. (c) The side and top views of Blue-P, Gray-As, β -AsP, and our newly predicted I-, II-, IV-, and V-AsP monolayers.

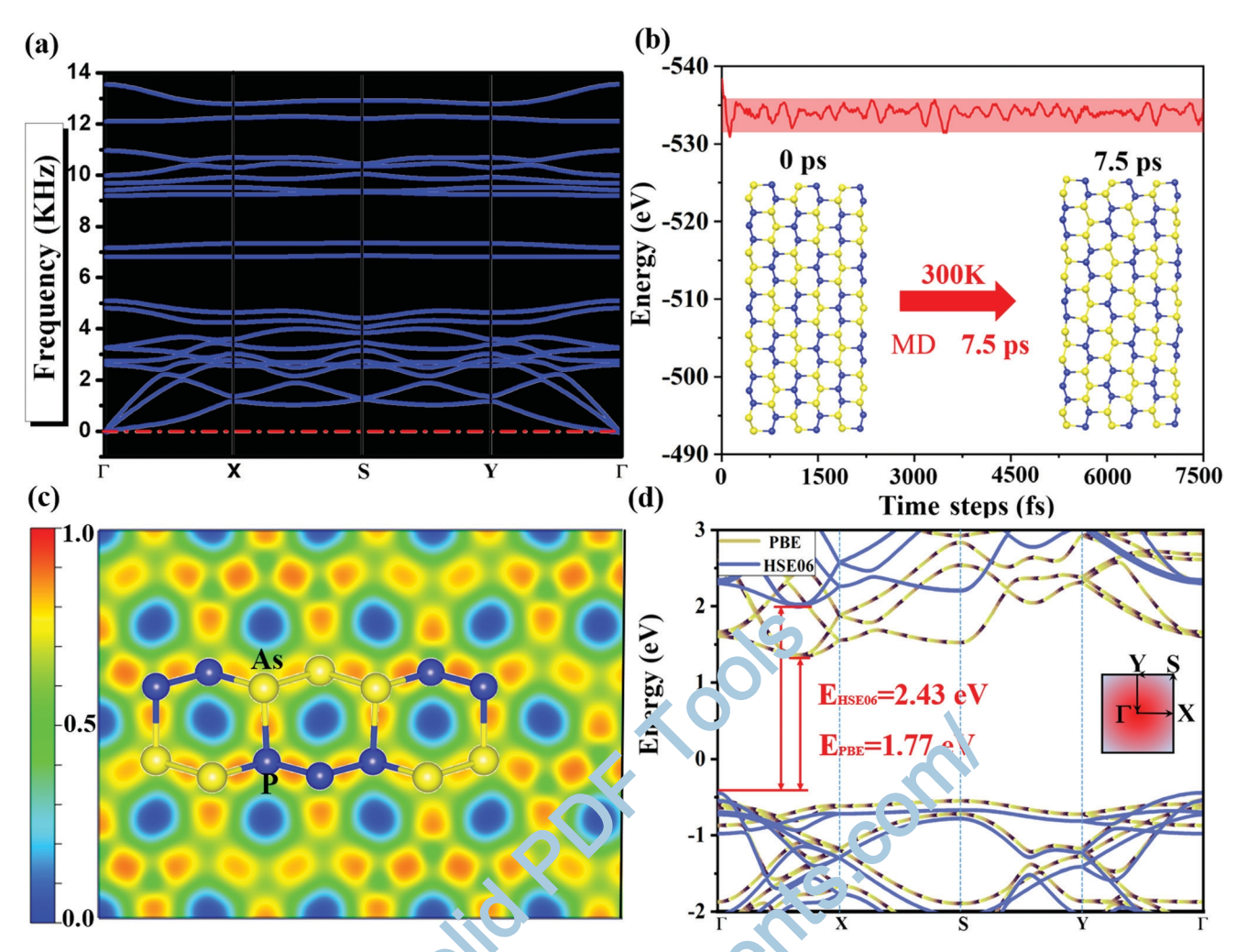


Fig. 2 (a) The calculated phonon spectrum for t'e i AsP monolayer, (b) the evolution of total energy and the structures of the I-AsP monolayer from AIMD simulations at T = 300 K, (c) ELF man silved perpendicular to the (0°) crection for the I-AsP monolayer, and (d) the electronic band structures of the I-AsP monolayer at PBE and HS .06 levels of theory. High syn. ne. y k points in the first Brillouin zone: Γ (0, 0, 0), χ (0.5, 0, 0), S (0.5, 0.5, 0) and Y (0, 0.5, 0).

temperature increases up to 750 K, the monolayer stackies start to break down and gradually lose their structural integrity (Fig. S2†).

Significantly, adopting an alloying strategy ent experiments have synthesized limited-layer black As, $_xP_x$ alloys with different and tunable compositions $(0.17 \le x \le 1)$ at elevated temperatures. 18,19 We are aware that the experimental synthesis of black $As_{1-x}P_x$ alloys is a gely affected by temperature.58 Since our AIMD simula ions suggest that I-AsP is not stable at 750 K, we followed a different route to prepare I-AsP in this study. Very recently, Cui et al. 59 proposed a novel kinetic pathway for fa rivating Blue-P via an epitaxial growth process; Zhang et au. 15 experimentally realized a molecular beam epitaxial, ro, th of Blue-P on Au(111) using black P as a precursor. Meanwhile, Chen et al. 16 successfully grew quasifree-standing Blue-P on Te-functionalized Au(111). These remarkable experimental achievements pave a way to the synthesis for Blue-AsP (I-AsP).

Electronic properties and tunable band gap engineering

To understand the chemical bonding, the electron localization function (ELF) and the corresponding partial densities of states (DOS) of the I-AsP monolayer were calculated. In the ELF (Fig. 2c), abundant electrons are tightly localized between adjacent atoms, revealing the strong covalent electron states of the σ bond formed by the sp³-hybridized orbitals of As and P atoms. The calculated DOS of the I-AsP monolayer (Fig. S3†) has strongly overlapping s-p orbitals for As and P atoms, confirming these covalent bonding characteristics.

The I-AsP monolayer is semiconducting with a quasi-direct band gap (Fig. 2d). The valence band maximum (VBM) occurs at the Γ point, while the conduction band minimum (CBM) lies between the Γ and X points, and is only slightly higher in energy than the Γ point. Such a weak indirect band gap is advantageous for photovoltaic applications (see below), and also permits strong absorption and high electron mobilities,

Paper Nanoscale

as reported in the InP_3 monolayer and some hybrid perovskites. ^{60,61} Particularly, the band gap of the I-AsP monolayer (1.77 eV at PBE and 2.41 eV at HSE06) is well-suited to photovoltaic applications.

Compressive or tensile strains have been demonstrated, both experimentally and theoretically, as an effective method to modulate the electronic band structures.⁶² Meanwhile, 2D materials can easily bear a certain strain effect, which can be operated through a lattice mismatch on a substrate or by mechanical loading in experiments.²⁰ Therefore, we have examined the effect of strain on the band structures of the I-AsP monolayer. An imposed uniaxial strain is defined as $\delta = \Delta l/l_0$, where Δl is the change of the lattice constant and l_0 is the lattice constant of the rectangle supercell. The dependence of the band gap on the in-plane stretching along the zigzag direction and the armchair direction was calculated under strain from -15% to 15% (Fig. 3a), respectively. Interestingly, the band gaps of the I-AsP monolayer decrease gradually with either compressive or tensile strains, which differs from the monotonic trend from compression to tension as found in the case of Black-P.3 This feature can be attributed to Mexican-hat-like⁶³ flat valence bands, which render sharp peaks in the density of states (DOS) and van Hove singularities (VHSs) with $\frac{1}{\sqrt{E}}$ divergence near the Fermi level as suggested by Fig. S3,† akin to Blue-P14 and InP3 monolayers.64 Such electronic states bring about a non-monotonic response ga the VBM or CBM to various strains and lead to the unusual bond gap trend from compression to tension.

Moreover, the structures of the I-AsP monolayer can change into a multilayer by a van der Waals (vdW) stacking strategy. The possible stacking patterns for the bilayer (2L) and trilayer (3L) I-AsP are presented in Fig. S4† and their cohesive-energy differences are evaluated (Tables S2 and S3†). Among these, the AB and ABC stacking are the ground state structures, which are the same as for the Blue-P and Gray-As. Adopting the stable 2L (AB) and 3L (ABC) stackings, we further calculated the layer-dependent band gap of I-AsP sheets (Fig. 3b). We found that the band gap of I-AsP can also be tuned by increasing the number of layers, and shows a monotonic decrease with increasing the I-AsP layers.

Interestingly, the band gap on the in-plane stretching along the zigzag direction and biaxial strain can be tuned to have direct character (Fig. S5†). The I-AsP monolayer has an indirect-to-direct gap transition at the Γ point under tensile strains of ~13% along the zigzag direction (Fig. 3c) and under ~3.8% biaxial compressive strain (Fig. 3d), respectively. Notably, the character of the direct band gap can be fixed and the gap value changed from ~0 eV to ~2 eV by biaxial strain from 3.8% to 6% under the PBE level (Fig. S5†). These band gap characteristics for the I-AsP monolayer, in respense to tensile strains, are quite similar to those of Blue-P and Gray-As. ¹⁴ Such a strain- uned direct band gap has a clear advantage for its potential photovoltaic applications, as electronic excitation λ comes possible at lower phonon energy.

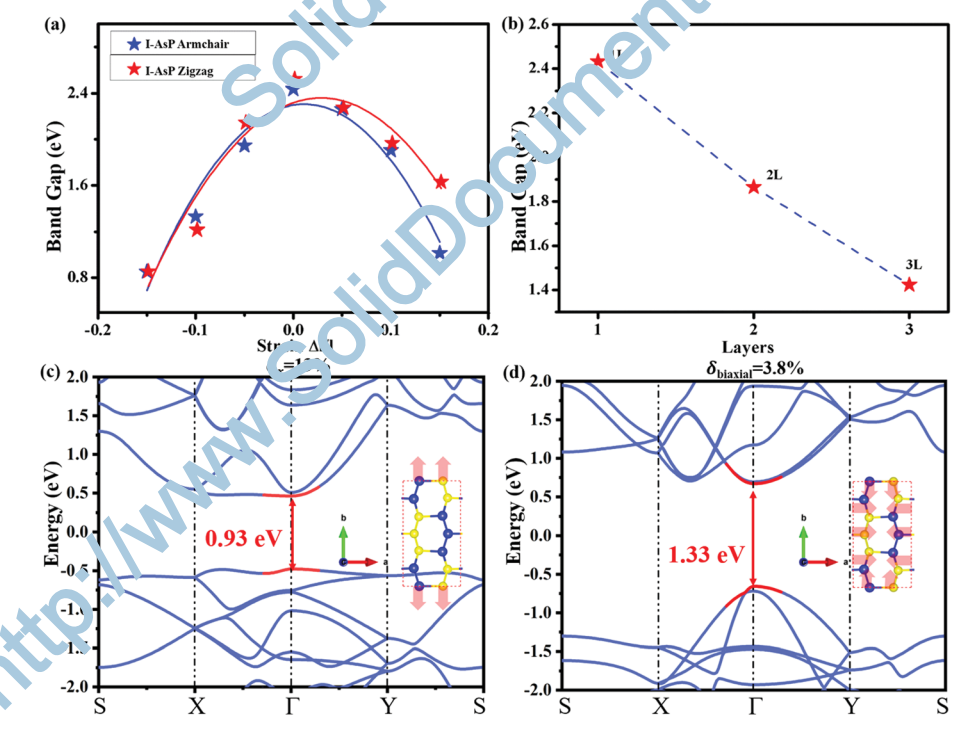


Fig. 3 (a) Dependence of the band gap of the I-AsP monolayer on the in-layer strain from -15% to 15%, (b) the layer-dependent band gap of I-AsP. (c-d) The indirect-direct semiconductor transition is triggered by 13% tensile strain along the zigzag direction (c) and 3.8% biaxial compressive strain (d), respectively.

Carrier mobilities of the I-AsP monolayer

We note that the conduction bands in the calculated band structure of the I-AsP monolayer are rather dispersive, which implies a high electron mobility. Thus, we have theoretically investigated the carrier mobilities of the I-AsP monolayer along the zigzag and armchair directions. According to the deformation potential (DP) proposed by Bardeen and Shockley, 65 under the effective mass (m^*) approximation, the analytical expression of acoustic-phonon-limited carrier mobility (μ) in 2D materials is given as

$$\mu = \frac{e\hbar^3 C_{2\mathrm{d}}}{k_{\mathrm{B}} T m^* m_{\mathrm{d}} (E_{2\mathrm{d}}^*)^2}$$

in which $k_{\rm B}$ is the Boltzmann constant, e is the electron charge, and the temperature T is set to 300 K. The average effective mass (m_d) is equal to $m_d = \sqrt{m^a m^b}$. The effective mass m^* (m^a and m^b) of holes and electrons is calculated based on the data about the band structure (VBM for holes and CBM for electrons along Γ -X and Γ -Y for the rectangle cell) and is given by the equation:

$$m^* = \hbar^2 \left[\frac{\partial^2 E(k)}{\partial k^2} \right]^{-1}$$

where k is the wave vector, and E(k) is the energy corresponding to k. $C_{2d} = [\partial^2 E/\partial \delta^2]/S_0$ and $E_{2d}^* = \partial \Delta E/\partial \delta$ are the ir plane stiffness with the longitudinal strain and the defor mation potential as the change of band edges in VB. 1 fo holes and CBM for electrons when in-plane stairs are employed along the zigzag and armchair directions, respectively. S_0 and ΔE are the area of the equilibrium up reell and the value of CBM (VBM) relative to the vacuum anargy, respectively. $\delta = \Delta l/l_0$ and E is the total energy.

Related data are given in Fig. S6. The calculated deformation potential constant E_{2d}^* , the elastic modulus C_{2d} , the effective mass m^* and mobility μ of electrons and holes along zigzag and armchair directions are summarized in Table ... Except for the 2D elastic modulus C, most quantities are of moderate magnitudes and are anisotropic along the zirrag and armchair directions. These features are rather s muar to Blue-P and Gray-As: the directional 2D elastic magness C for the I-AsP, Blue-P, and Gray-As all are relativity is tropic, which may result from their similar planar isotropic hexatomic rings. Comparing the calculated m^* values for I AsP, Blue-P, and

Grav-As, the effective mass m^* of electrons are within an order of magnitude, but are smaller than the corresponding value for holes, which can be understood by the very flat valence band and the more dispersive conduction band. As expected, the distinctively dispersive conduction bands lead to ultrahigh electronic mobility in both zigzag and armchair directions. The calculated electron mobility for the I-AsP monolayer is up to $\sim 7.4 \times 10^4$ cm² V⁻¹ s⁻¹, which far surpasses that of Blue-P $(\sim 4.7 \times 10^{2} \text{ cm}^{2} \text{ V}^{-1} \text{ s}^{-1})$, ¹⁷ Gray-As $(\sim 4.74 \times 10^{3} \text{ cm}^{2} \text{ V}^{-1} \text{ s}^{-1})$, ²⁹ and the α -AsP ($\sim 1.4 \times 10^4 \text{ cm}^2 \text{ V}^{-1} \text{ s}^{-1}$), ³⁸ and suggests its ability for high charge carrier transfer in photovoltaic applications. Moreover, the carrier mobilities of the bilayer and trilayer I-AsP were evaluated (Table S4†). Our calculations indicate that μ strongly depends on the number of layers and are anisotropic in the zigzag (x) and armchair (y) directions. Electron mobilities in the x direction and holes mobility along the x or y direction are increasing with the number of layers, which was expected already from the change of the effective mass and the deformation potential constant in their band structure (Fig. S8 and S9†).

Optical preparties of the I-AsP monolayer

We have ca culated absorption properties based on the dielectr'e 1 inction $\varepsilon(\omega) = \varepsilon_1(\omega) + i\varepsilon_2(\omega)$, where ω is the frequency. The absorption coefficient $\alpha(\omega)$ was calculated using

$$\alpha(\omega) = \sqrt{2}\omega \Big(\sqrt{\varepsilon_1}^2(\omega) + \varepsilon_2^2(\omega) - \varepsilon_1(\omega)\Big)^{1/2}$$

where ε_1 is the real part of the complex dielectric function, which could be sained from ε_2 using the Kramer-Kronig relationship, ϵ_2 is Jefined as:^{5,6}

$$egin{aligned} \mathcal{L}(\omega) &= rac{4\pi^2 e^2}{\Omega} \!\lim_{q o 0} rac{1}{q^2} \!\sum_{\mathrm{c,v},ec{k}} 2w_k \delta(arepsilon_{\mathrm{ck}} - arepsilon_{\mathrm{vk}} - \omega) \ & imes \langle \mu_{\mathrm{ck} + arepsilon_{a}} | \mu_{\mathrm{vk}}
angle
angle \langle \mu_{\mathrm{ck} + arepsilon_{eta}} | \mu_{\mathrm{vk}}^*
angle \end{aligned}$$

where α and β refer to the x and y directions, and Ω is the volume of the unit cell. The indices c and v refer to the conduction and valence band states, respectively. μ_{ck} corresponds to an eigenstate with wave vector k.

We have calculated the absorption coefficients of I-AsP and compared them with those of Blue-P and Gray-As (Fig. 4a). The overall absorption coefficients along the in-plane directions (zigzag and armchair directions) of the I-AsP monolayer are

Table 1 Calculated effective mass (m_0) , deformation potential constant (E_d) , 2D elastic modulus C^{2D} , and mobility (μ) for electron (e) and holes (h) along zigzag (y) and armchair (x, a rections

2D structures		$\frac{1}{n_{\lambda}^{*}}/m_{\lambda}$	m_y^*/m_0	$C_x^{\mathrm{2D}} \left(\mathrm{N \ m}^{-1} \right)$	$C_y^{\mathrm{2D}} \left(\mathrm{N \ m}^{-1} \right)$	E_{d}^{x} (eV)	$E_{\rm d}^{\rm y}$ (eV)	$\mu_x (\text{cm}^2 \text{V}^{-1} \text{s}^{-1})$	$M_y \text{ cm}^2 \text{ V}^{-1} \text{ s}^{-1}$
I-AsP	e	0, 1	0.12	62.51	63.18	2.30	1.08	17.50×10^3	74.49×10^{3}
	y za	0.10	0.46	62.51	63.18	10.18	2.13	540	2550
Gray-As ^a	2	0.13	0.13	55.50	55.50	3.9	3.9	4.74×10^{3}	4.74×10^{3}
	h	0.53	0.53	55.50	55.50	1.7	1.7	1460	1460
Blue-P ^b	e	0.94	0.14	78.09	78.19	3.20	2.09	4.7×10^{2}	50
	h	3.48	0.83	78.09	78.19	0.61	11.85	1710	60

^a Ref. 29. ^b Ref. 17.

Paper Nanoscale

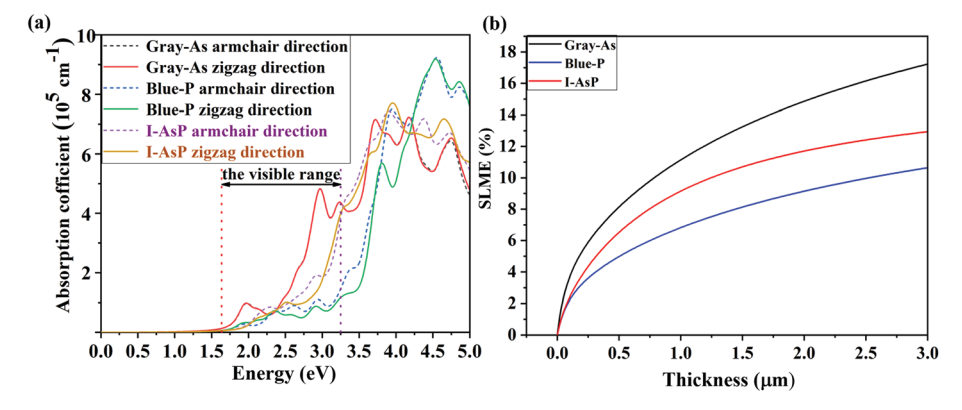


Fig. 4 (a) The calculated light absorption spectra for the Gray-As, Blue-P, and the I-AsP monolayer. (b) The theoretical photovoltaic efficiency (SLME) as a function of slab thickness for the I-AsP sheets compared with Gray-As and Blue-P.

larger (10⁵ cm⁻¹) than those of Blue-P, and comparable to those of Gray-As. Their absorption coefficients along zigzag and armchair directions are nearly equal for every light region. These relatively isotropic in-plane directional absorption coefficients reflect their planar and rather isotropic strings in the structure. These outstanding optical performances of the I-AsP monolayer suggest that it may be a very promising material for efficient photovoltaic solar cell applications or in optoelectronic devices.

The I-AsP sheets as a photovoltaic material in solar cells

The above calculations show that our newly predicted in Normannolayer has a quasi-direct band gap (2.41 eV) similar to that of Blue-P (~2.62 eV) and Gray-As (~2.49 eV), and the quasi-

direct band gap is tunable to a direct and optimal gap for photovoltaic applications. The outstanding optical properties further suggest its promise as an efficient photovoltaic material for use in solar cells. Note that the photovoltaic efficiency in the practical solar cells also relies on the thickness of the LASP sheets. Thus, we theoretically calculated the photomeric efficiencies of the I-ASP sheets, by calculating the spectroscopic limited maximum efficiency (SLME) based on the improved Shockley-Quais er model. 66 This was calculated as a function of the trickness by noting the absorption coefficients and the thickness of the sheets. This simulation was performed under the standard AM1.5G solar spectrum at room temperature, and compared with those of Blue-P and Gray-As.

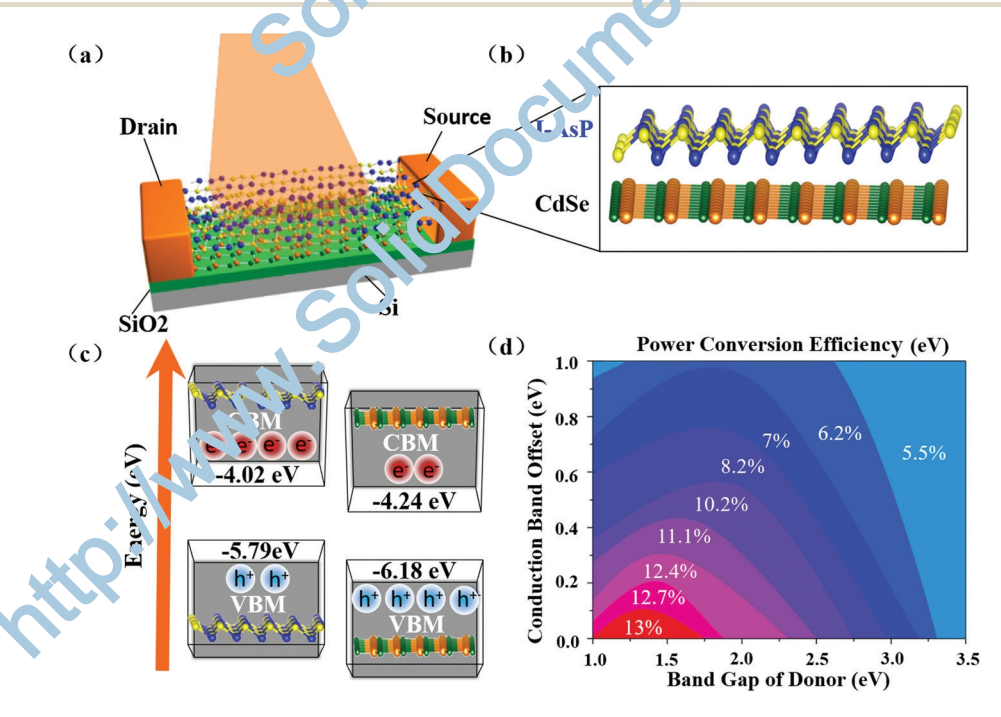


Fig. 5 (a) Schematic of the I-AsP/CdSe heterostructure-based solar cell. (b) The optimized structure of the I-AsP/CdSe heterostructure. (c) Schematic drawing of the type-II band I-AsP/CdSe heterostructure. (d) Simulated PCE of the heterostructure made by I-AsP/CdSe materials.

Nanoscale Paper

Notably, the SLME of I-AsP sheets is higher than that of Blue-P and close to that of Gray-As for any given thickness (Fig. 4b). Their photovoltaic efficiency generally increases as the thickness of these sheets is augmented over the 0-3.0 µm range. For example, 30 nm-thick I-AsP sheet-based cells can have a photovoltaic efficiency up to ~12%, higher than the Blue-P, and comparable to that of c-Si⁶⁷ (\sim 10%).

Furthermore, we constructed a type-II band solar cell of the I-AsP/CdSe heterostructure (Fig. 5a), where I-AsP and CdSe are donor and acceptor materials (Fig. 5b), respectively, based on the CBM (-4.02 eV) and the VBM (-5.79 eV) for I-AsP as well as the CBM (-4.32 eV) and the VBM (-6.12 eV) for CdSe⁶⁸ (Fig. 5c). Subsequently, the energy conversion efficiency (PCE) η of the I-AsP/CdSe heterostructure is calculated according to:49

$$\eta = \frac{J_{\text{SC}}V_{\text{OC}}\beta_{\text{FF}}}{P_{\text{solar}}}$$

$$= \frac{0.65(E_{\text{g}}^{\text{d}} - \Delta E_{\text{c}} - 0.3) \int_{E_{\text{g}}^{\text{d}}}^{\infty} P(h\omega)d(h\omega)}{\int_{0}^{\infty} P(h\omega)d(h\omega)}$$

in which J_{sc} , V_{oc} , β_{FF} and P_{solar} are the short circuit current, the maximum open circuit voltage in eV units, the band-fill factor $(\beta_{\rm FF} = 0.65)$, and the incident solar flux $(P_{\rm solar} = 1000 \text{ W m}^{-2})$, respectively. In detail, $J_{\rm sc}$ is the integral $\int_{E_{\alpha}^{\sigma}}^{\infty} P(\hbar\omega) d(\hbar\omega)$ in the limit of 100% external quantum efficiency (EQE), 69 P_{solar} is obtained from the integral $\int_0^\infty P(\hbar\omega)d(\hbar\omega)$ for the AM1.5 sol τ flux $P(\hbar\omega)$ (stated in W m⁻² eV⁻¹), and $V_{\rm oc}$ is derived from the $(E_{\rm g}^{\rm d} - \Delta E_{\rm c} - 0.3)$ term, where $E_{\rm g}^{\rm d}$ is the band gap of the denote I-AsP and ΔE_c is the energy difference between CL of the donor I-AsP and the acceptor CdSe.

As can be seen in Fig. 5d, the I-AsP/CdS 1 e ar structure solar cell can possess a PCE as high as ~13% which is much higher than the best value (~9%) of existing colar cells, 70 and competitive with the nanocarbon-based photovoltaics $(9-13\%)^{71}$, and close to the g-SiC₂ systems $(12-20\%)^{72}$ and the proposed MoS₂/phosphorene heterostructure recently (16–18%). 73,74 These simulations confirmed that the sheets can be used as a photovoltaic material in solar ce is with a superior photovoltaic efficiency.

Conclusion

In summary, we have identified the low ring energy structures of the As_xP_{1-x} monolayer in the 21 space based on the PSO algorithm approach combined in hab initio calculations, and confirmed that the As: ? = 1:1 composition is thermodynamically most favorable among all the examined stoichiometries. At this 1.1 composition, a series of energetically favored Blue-AsP n.on layers (x-AsP, x = I, II, III, IV, V), sharing similar honeycome structures with Blue-P, were predicted for the first time. The lowest-energy I-AsP monolayer has a quasidirect band gap (2.41 eV) and Mexican-hat like flat bands near the Fermi energy, which lead to a nonmonotonic electronic response to compressive and tensile strains. Remarkably, an

indirect-to-direct gap transition can occur under tensile strains of ~13% along the zigzag direction or at ~3.8% biaxial compressive strain. Moreover, the I-AsP monolayer possesses extraordinary electronic mobility up to $\sim 7.4 \times 10^4 \text{ cm}^2 \text{ V}^{-1} \text{ s}^{-1}$, and absorption coefficients (×10⁵ cm⁻¹) far surpassing those of Blue-P across the entire visible solar spectrum. These advantages demonstrate it as a very promising material for highefficiency solar cells. As indicated by our simulations, 30 nmthick I-AsP sheet-based cells can have a photovoltaic efficiency up to ~12% and the I-AsP/CdSe heterostructure solar cell can possess a PCE as high as ~13%. All these data strongly suggest that the I-AsP sheet is a very promising photovoltaic material for use in solar cells.

Author contributions

Yuanzheng Chen and Zhongfang Chen conceived and designed this work; Xinyong Cai, Jiao Chen and Xiumei Li performed the related calculations; Xinyong Cai, Shouhui Zhu and Li Tao prepared the figures; Bai Sun, Hongyan Wang, Yuxiang N. nu Wang, Yanchao Wang, and Jian Lv contributed import at discussions; the manuscript was written by Yuantheng Chen and Zhongfang Chen; Xiaolei Feng and on A. T. Redfern discussed related results and reviewed the manuscript. All authors approved the final version of the manuscript.

Conflicts crinterest

The authors 'lec' are no competing financial interest.

Acknowledgements

This work was supported in China by the National Natural Science Foundation of China (No. 11604270 and 11704050), the Fundamental Research Funds for the Central Universities (2682017CX052; 2018GF08), and the Sichuan Science and Technology program (2017JY005), and in USA by the NSF-CREST Center for Innovation, Research and Education in Environmental Nanotechnology (CIRE2N) (Grant Number HRD-1736093). S. A. T. R. acknowledges the support of the UK Natural Environment Research Council under grant NE/ P012167/1.

References

- 1 R. Hultgren, N. S. Gingrich and B. E. Warren, J. Chem. Phys., 1935, 3, 351-355.
- 2 S. Zhang, S. Guo, Z. Chen, Y. Wang, H. Gao, J. Gomez-Herrero, P. Ares, F. Zamora, Z. Zhu and H. Zeng, Chem. Soc. Rev., 2018, 47, 982-1021.
- 3 H. Liu, A. T. Neal, Z. Zhu, Z. Luo, X. Xu, D. Tománek and P. D. Ye, ACS Nano, 2014, 8, 4033-4041.

Paper

- 4 H. O. Churchill and P. Jarillo-Herrero, Nat. Nanotechnol., 2014, 9, 330-331.
- 5 M. Wu, H. Fu, L. Zhou, K. Yao and X. C. Zeng, Nano Lett., 2015, 15, 3557-3562.
- 6 J. Guan, Z. Zhu and D. Tomanek, Phys. Rev. Lett., 2014, 113, 226801.
- 7 H. Wang, X. Li, Z. Liu and J. Yang, Phys. Chem. Chem. Phys., 2017, 19, 2402-2408.
- 8 G. Schusteritsch, M. Uhrin and C. J. Pickard, Nano Lett., 2016, 16, 2975-2980.
- 9 T. Zhao, C. Y. He, S. Y. Ma, K. W. Zhang, X. Y. Peng, G. F. Xie and J. X. Zhong, J. Phys.: Condens. Matter, 2015, 27, 265301.
- 10 W. H. Han, S. Kim, I. H. Lee and K. J. Chang, J. Phys. Chem. Lett., 2017, 8, 4627-4632.
- 11 H. Wang, X. Li, P. Li and J. Yang, Nanoscale, 2017, 9, 850-
- 12 Y. Zhang, Z. F. Wu, P. F. Gao, D. Q. Fang, E. H. Zhang and S. L. Zhang, Phys. Chem. Chem. Phys., 2017, 19, 2245-2251.
- 13 P. Li and W. Luo, Sci. Rep., 2016, 6, 25423.
- 14 Z. Zhu and D. Tománek, Phys. Rev. Lett., 2014, 112, 176802.
- 15 J. L. Zhang, S. Zhao, C. Han, Z. Wang, S. Zhong, S. Sun, R. Guo, X. Zhou, C. D. Gu, K. D. Yuan, Z. Li and W. Chen, Nano Lett., 2016, 16, 4903-4908.
- 16 C. Gu, S. Zhao, J. L. Zhang, S. Sun, K. Yuan, Z. Hu, C. Har., Z. Ma, L. Wang, F. Huo, W. Huang, Z. Li and W. Chen Nano, 2017, 11, 4943-4949.
- 17 J. Xiao, M. Long, X. Zhang, J. Ouyang, H. Xu and Y. Gao, Sci. Rep., 2015, 5, 9961.
- 18 B. Liu, M. Kopf, A. N. Abbas, X. Wang, Q. Guo, Y. ia, F. Xia, R. Weihrich, F. Bachhuber, F. Pielnhofer, H. Wang, R. Dhall, S. B. Cronin, M. Ge, X Fang, T. Nilges and C. Zhou, Adv. Mater., 2015, 27, 4423 .42).
- 19 O. Osters, T. Nilges, F. Bachhuper, F. Pielnhofer, R. Weihrich, M. Schoneich and P. Schmidt, Angew. Chem., Int. Ed., 2012, 51, 2994-2997.
- 20 C. Kamal and M. Ezawa, Phys. Rev. B: Condens. Mat. 21 Mater. Phys., 2015, 91, 085423.
- 21 D. Kecik, E. Durgun and S. Ciraci, Phys. Rev I: Coldens. Matter Mater. Phys., 2016, 94, 205410.
- 22 J. Carrete, L. J. Gallego and N. Mingo, J. Phy. Chem. Lett., 2017, 8, 1375-1380.
- 23 M. J. Kelly and D. W. Bullett, Solid Star Commun., 1976, 18, 593-595.
- 24 B. Peng, H. Zhang, H. Shao, K. Yu, G. Ni, J. Li, H. Zhu and C. M. Soukoulis, J. Mater Ch. A, 2018, 6, 2018–2033.
- 25 Y. Chen, C. Chen, R. Yealholer, H. Liu, Z. Yuan, L. Jiang, J. Suh, J. Park, C. Ko, H. S. Choe, J. Avila, M. Zhong, Z. Wei, J. Li, S. Li, H. Goo, Y. Jiu, J. Analytis, Q. Xia, M. C. Asensio and J. Wu, Adv. Mator. 2018, 30, 1800754.
- 26 F. Ersan, E. Ak ürk and S. Ciraci, Phys. Rev. B: Condens. Matter Mater. Phys., 2016, 94, 245417.
- 27 S. Zhang, M. Xie, F. Li, Z. Yan, Y. Li, E. Kan, W. Liu, Z. Chen and H. Zeng, Angew. Chem., Int. Ed., 2016, 55, 1666-1669.

- 28 S. Ma, P. Zhou, L. Z. Sun and K. W. Zhang, Phys. Chem. Chem. Phys., 2016, 18, 8723-8729.
- 29 P. Jamdagni, A. Thakur, A. Kumar, P. K. Ahluwalia and R. Pandey, Phys. Chem. Chem. Phys., 2018, 20, 29939-29950.
- 30 H.-S. Tsai, S.-W. Wang, C.-H. Hsiao, C.-W. Chen, H. Ouyang, Y.-L. Chueh, H.-C. Kuo and J.-H. Liang, Chem. Mater., 2016, 28, 425-429.
- 31 Z. Zhu, J. Guan and D. Tománek, Phys. Rev. B: Condens. Matter Mater. Phys., 2015, 91, 161404(R).
- 32 S. Zhang, Z. Yan, Y. Li, Z. Chen and H. Zeng, Angew. Chem., Int. Ed. Engl., 2015, 54, 3112-3115.
- 33 M. Amani, E. Regan, J. Bullock, G. H. Ahn and A. Javey, ACS Nano, 2017, 11, 11724-11731.
- 34 S. Yuan, C. Shen, B. Deng, X. Chen, Q. Guo, Y. Ma, A. Abbas, B. Liu, R. Haiges, C. Ott, T. Nilges, K. Watanabe, T. Taniguchi, O. Sinai, D. Naveh, C. Zhou and F. Xia, Nano Lett., 2018, 18, 3172-3179.
- 35 H. Krebs, W. Holz and K. H. Worms, Ber., 1957, 90, 1031-1037.
- 36 I. Karakaya and W. T. Thompson, J. Phase Equilib. Diffus., 1991, 12, 543-346.
- 37 Z. Zhu, J. Guan and D. Tomanek, Nano Lett., 2015, 15, 6042 60 16.
- 3° M. X e, S. Zhang, B. Cai, Y. Huang, Y. Zou, B. Guo, Y. Gu and H. Zeng, Nano Energy, 2016, 28, 433-439.
- 39 F. Shojaei and H. S. Kang, J. Phys. Chem. C, 2015, 119, 20210-20216.
- 40 Y. Wang, J. Lv, L. Zhi, and Y. Ma, Comput. Phys. Commun., 2012, 183, 2063-2070.
- 41 Y. Wang, M. (Ga), J. Lv, L. Zhu, K. Yin, H. Liu and Y. Ma, J. Chem. Flys., 2012, 137, 224108.
- 42 Y. Chen. Y. Xi, W.-L. Yim, F. Peng, Y. Wang, H. Wang, Y. Ma, C. Liu, C. Sun, C. Ma, Z. Chen and H. Berger, J. Prys. Chem. C, 2013, 117, 25677-25683.
- 43 Y Chen, F. Peng, Y. Yan, Z. Wang, C. Sun and Y. Ma, 7. Phys. Chem. C, 2013, **11**7, 13879–13886.
- 44 Z. Wang, Y. Li, H. Li, I. Harran, M. Jia, H. Wang, Y. Chen, H. Wang and N. Wu, J. Alloys Compd., 2017, 702, 132–137.
- 45 Y. Chen, X. Cai, H. Wang, H. Wang and H. Wang, Sci. Rep., 2018, 8, 10670.
- 46 X. Li, H. Li, J. Chen, X. Cai, H. Wang, Z. Lao, B. Sun, L. Tao and Y. Chen, J. Alloys Compd., 2019, 778, 588-592.
- 47 I. Harran, Y. Chen, H. Wang, H. Li, Y. Li and L. Tao, J. Alloys Compd., 2017, 710, 267-273.
- 48 L. Zhao, W. Yi, J. Botana, F. Gu and M. Miao, J. Phys. Chem. C, 2017, **121**, 28520–28526.
- 49 P. E. Blöchl, Phys. Rev. B: Condens. Matter Mater. Phys., 1994, 50, 17953-17979.
- 50 G. Kresse and D. Joubert, Phys. Rev. B: Condens. Matter Mater. Phys., 1999, 59, 1758-1775.
- 51 G. Kresse and J. Furthmüller, Phys. Rev. B: Condens. Matter Mater. Phys., 1996, 54, 11169-11186.
- 52 M. Dion, H. Rydberg, E. Schröder, D. C. Langreth and B. I. Lundqvist, Phys. Rev. Lett., 2004, 92, 246401.
- 53 J. Heyd, G. E. Scuseria and M. Ernzerhof, J. Chem. Phys., 2003, 118, 8207-8215.

Nanoscale Paper

- 54 A. Togo and I. Tanaka, Scr. Mater., 2015, 108, 1-5.
- 55 W. Yu, C.-Y. Niu, Z. Zhu, X. Wang and W.-B. Zhang, J. Mater. Chem. C, 2016, 4, 6581-6587.
- 56 H. Yin, J. Gao, G.-P. Zheng, Y. Wang and Y. Ma, J. Phys. Chem. C, 2017, 121, 25576-25584.
- 57 J. Ahn, I. Hong, Y. Kwon, R. C. Clay, L. Shulenburger, H. Shin and A. Benali, Phys. Rev. B: Condens. Matter Mater. Phys., 2018, 98, 085429.
- 58 A. Ektarawong, S. I. Simak and B. Alling, Phys. Rev. B: Condens. Matter Mater. Phys., 2017, 96, 024202.
- 59 J. Zeng, P. Cui and Z. Zhang, Phys. Rev. Lett., 2017, 118, 046101.
- 60 N. Miao, B. Xu, N. C. Bristowe, J. Zhou and Z. Sun, J. Am. Chem. Soc., 2017, 139, 11125-11131.
- 61 F. Zheng, L. Z. Tan, S. Liu and A. M. Rappe, Nano Lett., 2015, 15, 7794-7800.
- 62 K. He, C. Poole, K. F. Mak and J. Shan, Nano Lett., 2013, 13,
- ad X. C. Ze.

 Lu, H. Guo, L. Wan
 2014, 6, 4566-4571. 63 L. Seixas, A. S. Rodin, A. Carvalho and A. H. Castro Neto,

- 64 N. Miao, B. Xu, N. C. Bristowe, J. Zhou and Z. Sun, J. Am. Chem. Soc., 2017, 139, 11125-11131.
- 65 J. Bardeen and W. Shockley, Phys. Rev., 1950, 80, 72-80.
- 66 L. Yu and A. Zunger, Phys. Rev. Lett., 2012, 108, 068701.
- 67 J. Lv, M. Xu, S. Lin, X. Shao, X. Zhang, Y. Liu, Y. Wang, Z. Chen and Y. Ma, Nano Energy, 2018, 51, 489-495.
- 68 J. Linghu, T. Yang, Y. Luo, M. Yang, J. Zhou, L. Shen and Y. P. Feng, Appl. Mater. Interfaces, 2018, 10, 32142-32150.
- 69 M. Bernardi, M. Palummo and J. C. Grossman, ACS Nano, 2012, 6, 10082-10089.
- 70 M. A. Green, Prog. Photovoltaics, 2017, DOI: 10.1002/pip.2876.
- 71 M. Bernardi, J. Lohrman, P. V. Kumar, A. Kirkeminde, N. Ferralis, J. C. Grossman and S. Ren, ACS Nano, 2012, 6,
- 72 L. J. Zhou, Y. F. Zhang and L. M. Wu, Nano Lett., 2013, 13, 5431-5436.
- 73 J. Dai and X. C. Zeng, J. Phys. Chem. Lett., 2014, 5, 1289-
- 74 N. Lu, H. Guo, L. Wang, X. Wu and X. C. Zeng, Nanoscale,